Journal of Applied Polymer Science

Preparation of a porous, magnetic, quaternary chitosan salt by preadsorption and desorption for azo dye adsorption from water

Conglu Zhang,[1] Lei Zhu,[2] Wei Li,[3] Xin Zheng[1]

[1]School of Pharmaceutical Engineering, Shenyang Pharmaceutical University, Shenyang 110016, People's Republic of China
[2]Institute of Resources and Civil Engineering, Northeastern University, Shenyang 110014, People's Republic of China
[3]School of Management, Shenyang Jianzhu University, Shenyang 110168, People's Republic of China
Correspondence to: C. Zhang (E-mail: twyla666@sina.com) and L. Zhu (E-mail: 4343722@qq.com)

ABSTRACT: A porous magnetic quaternary chitosan salt (pre-CS/EPTAC/Fe_3O_4) was successfully prepared via a kind of novel method of preadsorption and desorption. The physicochemical properties of pre-CS/EPTAC/Fe_3O_4 were characterized by Fourier transform infrared spectroscopy, scanning electron microscopy, and vibrating sample magnetometry. The adsorption of pre-CS/EPTAC/Fe_3O_4 for methyl orange (MO) showed much higher dye uptakes compared with Npre-CS/EPTAC/Fe_3O_4 without the preadsorption and desorption of MO, and the maximum adsorption capability for MO was 486.1 mg/g. Adsorption isotherms and adsorption kinetics were well fitted by the Freundlich isotherm model and the pseudo-second order model, respectively. Thermodynamic parameters, such as the standard free energy change, enthalpy change, and entropy change, were also calculated; this indicated that the adsorption was spontaneous and exothermic. The introduction of MO preadsorption and desorption into the process of preparation improved not only the adsorption of MO but also the adsorption of acid red 1 and orange G. Furthermore, pre-CS/EPTAC/Fe_3O_4 particles could be easily regenerated and remained almost constant (98.5%) for six cycles of adsorption and desorption. © 2016 Wiley Periodicals, Inc. J. Appl. Polym. Sci. **2016**, *133*, 43448

KEYWORDS: adsorption; kinetics; magnetism and magnetic properties; porous materials

Received 5 October 2015; accepted 18 January 2016
DOI: 10.1002/app.43448

INTRODUCTION

Azo dyes with properties of strong chemical stability, carcinogenesis, teratogenesis, and mutagenesis are major pollutants found in the effluents of the textile, plastic, article, leather, and cosmetic industries.[1] Many azo dyes are difficult to degrade because of their complex molecular structure and toxicity.[2,3] So, very small amounts of azo dyes not only cause greatly visible color in water bodies and disturb biological processes but also damage humans through mutagenic and carcinogenic effects.[4] To control water pollution and alleviate the water crisis, the removal of azo dyes has been paid more and more attention.

There are many kinds of techniques used for the treatment of dye-containing wastewater; these include biological treatment,[5] coagulation/flocculation,[6] chemical oxidation,[7] photocatalytic degradation,[8] ion exchange,[9] membrane filtration,[10] and adsorption.[11] Among the various techniques for dye removal from wastewater, adsorption is an effective and economical method because of its significant advantages of high flexibility, high efficiency, ease of operation, low operating cost, and lack of secondary pollution.[12] Many materials are used to adsorb dye wastewater, including active carbon,[13] resins,[14] zeolites,[15] and clays.[16] However, they have some disadvantages, such as a low adsorption capacity, long adsorption time, and separation inconvenience; this limits their applications in dye wastewater treatment.

Chitosan (CS), the *N*-deacetylated derivative of chitin, has a good biocompatibility, lack of toxicity, and biodegradability.[17] Because chitosan contains a large number of reactive hydroxyl (—OH) groups and amine (NH_2) groups, it exhibits good potential for anionic dye adsorption.[18,19] Nevertheless, as the adsorption material, chitosan is easy to lose, has a low mechanical strength, and has a poor regenerative ability in actual applications; this limits its widespread application.[20] The combination of chitosan or its derivatives with magnetic materials to a certain extent not only has excellent adsorption performance, but also will give the material certain mechanical strength, resistance to acid alkali and magnetic responsiveness.[21,22] Most of the literature has focused on the preparation of magnetic chitosan with ordinary crosslinking methods[23,24] and the surface modification of magnetic chitosan.[25,26] In our previous work,[27] magnetic quaternary chitosan particles were prepared through inverse suspension crosslinking

with Fe_3O_4 as the nucleus and glutaraldehyde as the crosslinking agent. The obtained magnetic quaternary chitosan material showed good performance in azo dye adsorption.

In this study, to improve the adsorption rate and adsorption capacity of the magnetic quaternary chitosan, a novel method of preadsorption and desorption of methyl orange (MO) was introduced into the process of preparation to gain a kind of porous magnetic quaternary chitosan material (pre-CS/EPTAC/Fe_3O_4). The preparation conditions, characterization, adsorption properties for MO in aqueous solution, and regenerability of pre-CS/EPTAC/Fe_3O_4 were studied and discussed. These research results could provide new insights into the preparation of advanced adsorbents.

EXPERIMENTAL

Materials

Chitosan, with a deacetylation degree of 94.68%, was purchased from Sinopharm Chemical Reagent Co., Ltd. (Shanghai, China). MO ($C_{14}H_{14}N_3SO_3Na$, (maximum absorption wavelength) $\lambda_{max} = 465$ nm), acid red 1 (AR1; $C_{18}H_{13}N_3$ NaO_8S_2, $\lambda_{max} = 505$ nm), and orange G (OG; $C_{16}H_{10}N_2Na_2O_7S_2$, $\lambda_{max} = 478$ nm) were purchased from Aladdin Reagent Co., Ltd. (Shanghai, China). All other chemical reagents were AR-grade reagents.

Preparation of Pre-CS/EPTAC/Fe_3O_4

Magnetic quaternary chitosan salt with preadsorption and desorption (pre-CS/EPTAC/Fe_3O_4) was prepared with a molar ratio of CS/EPTAC to Fe_3O_4 of 2:1 by the suspension crosslinking technique. Briefly, quaternary chitosan salt (CS/EPTAC, substitution degree = 0.98) was obtained by the reaction of chitosan with 2,3-epoxypropyl trimethylammonium chloride (EPTAC). Fe_3O_4 was prepared by coprecipitation.[28] Then, 0.2 g of CS/EPTAC was dissolved in 20 mL of distilled water, and a specified amount of Fe_3O_4 was added to this solution. After ultrasonic dispersion, a certain amount of MO was added and mixed for 1 h with stirring. Then, 50 mL of liquid paraffin and 2.5 mL of Span80 were added. The mixture was stirred for 30 min at 30 °C. Afterward, 3.0 mL of 50% v/v glutaraldehyde was added as a crosslinker, and the mixture was continuously stirred for 2.5 h at 60 °C. Finally, the magnetic quaternary chitosan salt was purified by magnetic field separation, washed with petroleum ether, ethanol, 0.1 mol/L sodium hydroxide solution, and distilled water in turn for the removal of the organic solvent and the residual MO. The products were dried *in vacuo* at 40 °C for 24 h. For comparison, CS/EPTAC/Fe_3O_4 without preadsorption and desorption (Npre-CS/EPTAC/Fe_3O_4) was prepared under identical conditions.

Characterization of Pre-CS/EPTAC/Fe_3O_4

The IR spectra of the samples were obtained with Fourier transform infrared (FTIR) spectroscopy (IFS55, Bruker, Germany), and the bands were changed from 4000 to 400 cm^{-1}. The surface morphology was analyzed with scanning electron microscopy (SEM; SSX-550, Shimadzu, Japan). The samples were coated with a thin gold layer. The magnetic properties were measured on with vibrating sample magnetometry (VSM; MPMS-7, Quantum Design) at room temperature (298 K).

Batch Adsorption Experiments

Adsorption Kinetics, Isotherms, and Thermodynamics. Batch adsorption experiments were carried out in 150-mL flasks. According to the previous research conclusions,[27] a certain concentration range of MO solutions at pH 3.0 were prepared. Then, 20 mg of adsorbent was immersed in a 50-mL solution. The solutions were oscillated in incubator shakers with a 150-rpm shaking speed. Thus, the adsorption kinetics and adsorption isotherms were studied at 298 K. At specified time intervals, the dye concentrations before and after adsorption were measured with an ultraviolet–visible spectrophotometer (UV2000, Unico Co., Ltd., China), and the adsorbents were collected by a magnetic field.

The equilibrium adsorption capacity (Q_e; mg/g) and removal rate (RR; %) were calculated according to eqs. (1) and 2[29]:

$$Q_e = \frac{(C_0 - C_e)V}{m} \quad (1)$$

$$RR = \frac{(C_0 - C_e)V}{m} \quad (2)$$

where C_0 and C_e are the initial and equilibrium concentrations of the dye in the solution (mg/L), respectively; V is the volume of the solution (mL); and m is the mass of adsorbent (g).

To obtain the thermodynamic parameters, adsorption experiments were conducted further at 298, 308, and 318 K. Meanwhile, the other conditions were unchanged. After adsorption for 120 min, the dye concentrations were measured via ultraviolet–visible spectrophotometry.

Adsorption for Other Azo Dyes. The adsorption for AR1 and OG were carried out in 150-mL flasks at 298 K. Dye solutions (50 mg/L) at pH 3.0 were prepared. Then, 20 mg of pre-CS/EPTAC/Fe_3O_4 and 20 mg of Npre-CS/EPTAC/Fe_3O_4 were immersed in 50-mL solutions, respectively. The solutions were oscillated in incubator shakers with a 150-rpm shaking speed for 120 min. At specified time intervals, the dye concentrations before and after adsorption were analyzed.

Recycling Experiments. The recovering and recycling experiments were performed at 298 K on the basis of the dye adsorption differences under different pH conditions. The dyes loaded by pre-CS/EPTAC/Fe_3O_4 were recovered with 20% NaOH aqueous solutions in incubator shakers with a 150-rpm shaking speed for 24 h. Then, the regenerated adsorbents underwent the next adsorption cycle. The adsorption–desorption of the MO dye was conducted for six cycles.

RESULTS AND DISCUSSION

Characterization

FTIR Analysis. The FTIR spectra of Npre-CS/EPTAC/Fe_3O_4 and pre-CS/EPTAC/Fe_3O_4 are shown in Figure 1. The FTIR spectra of in Figure 1(a) and 1(b) were very similar; this indicated that the preparation process did not destroy the major function groups of CS/EPTAC/Fe_3O_4. A characteristic strong and broad band appeared around 3400 cm^{-1} (in all of the spectra) corresponded to the combination of —OH stretching vibrations, N—H extension vibrations, and the interhydrogen bonds of polysaccharides. The spectra of Npre-CS/EPTAC/Fe_3O_4 exhibited the typical peak for the —CH_3 deformation vibrations of

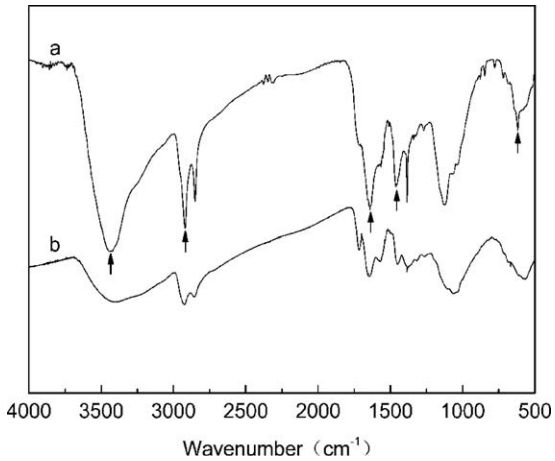

Figure 1. FTIR spectra of (a) Npre-CS/EPTAC/Fe_3O_4 and (b) pre-CS/EPTAC/Fe_3O_4.

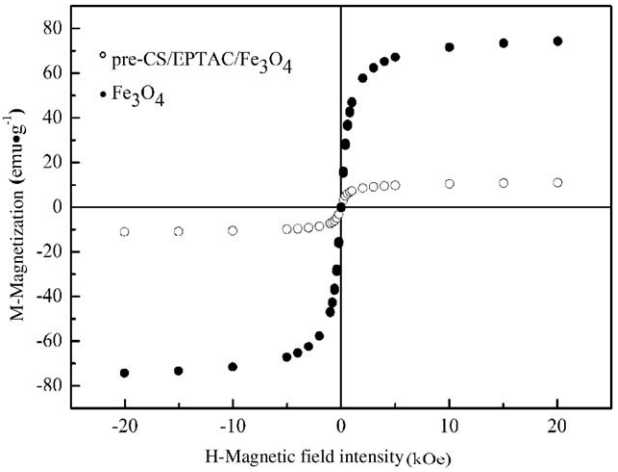

Figure 3. VSM of pre-CS/EPTAC/Fe_3O_4 and Fe_3O_4.

the quaternary ammonium group at 1460 and 1680 cm^{-1}; the peak at 2900 cm^{-1} was attributed to the —CH_3 stretching vibrations, and this basically coincided with the literature.[30] As shown in Figure 2(b), the intensities of these bands decreased after preadsorption and desorption: this result confirmed the interaction of MO and these groups. The peak appearing at a wavelength close to 568 cm^{-1} was assigned to Fe—O stretching vibrations in Fe_3O_4[31]; this confirmed the presence of Fe_3O_4 in pre-CS/EPTAC/Fe_3O_4.

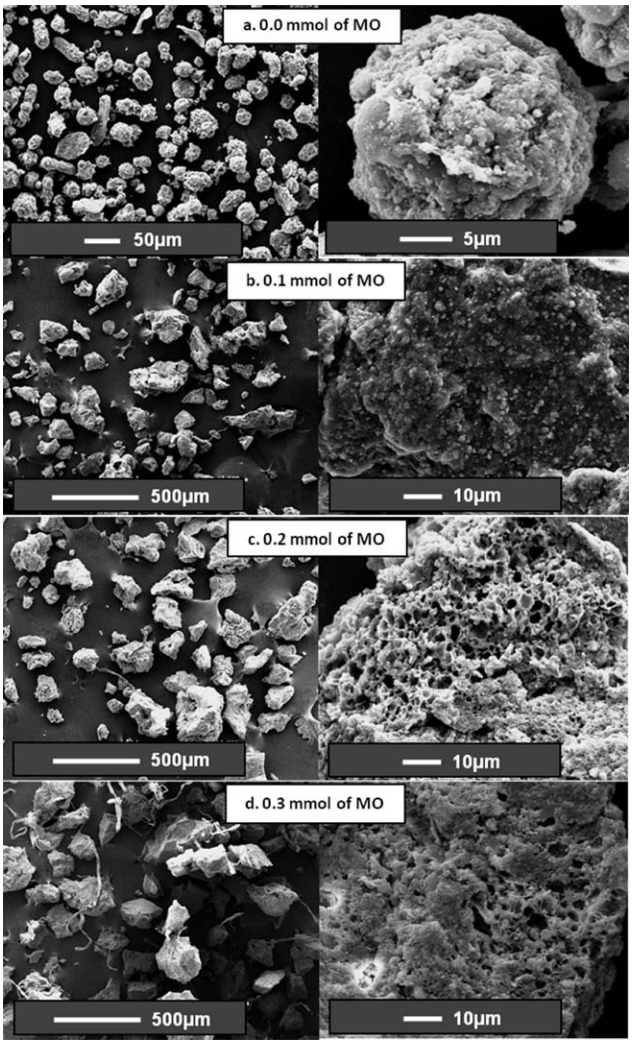

Figure 2. SEM of pre-CS/EPTAC/Fe_3O_4 with different amounts of preadsorption and desorption.

SEM Analysis. Figure 2 shows the SEM images of pre-CS/EPTAC/Fe_3O_4 under different amounts of MO of preadsorption and desorption. It was obvious that in the surface morphology of different adsorbents existed obvious differences with the changes in the amount of MO. Without MO [Fig. 2(a)], the sizes of the adsorbent particles were small, and the surface had no obvious cavities under an electron microscope. With the increase in MO amount, the adsorbent particles size also gradually increased, and the surfaces of particles had a lot of cavities. Among them, when the addition amount of MO was 0.2 mmol [Fig. 2(c)], the cavities on the particle surface were relatively regular and similar to a honeycomb. These adsorbent particles had a better dye adsorption performance, as discussed later.

VSM Analysis. Saturation magnetization is a crucial factor for successful magnetic separation. The saturation magnetization curves of Fe_3O_4 and pre-CS/EPTAC/Fe_3O_4 are displayed in Figure 3. Obviously, the zero remanence and coercivity were close to zero; this indicated that pre-CS/EPTAC/Fe_3O_4 and Fe_3O_4 were superparamagnetic. The saturation magnetization value of pre-CS/EPTAC/Fe_3O_4 (11.0 emu/g) at room temperature was lower than that of Fe_3O_4 (74.3 emu/g). The reason was ascribed to the low content of Fe_3O_4 in pre-CS/EPTAC/Fe_3O_4. Moreover, under the action of a magnetic field, pre-CS/EPTAC/Fe_3O_4 could have been completely attracted toward the magnet from the aqueous solution within a few seconds. The result suggests that in comparison with the adsorbent separated from water by gravity, pre-CS/EPTAC/Fe_3O_4 showed significantly improved the separation and collection properties with a magnetic field.

Removal of MO and Other Azo Dyes

Adsorption Comparisons of the Adsorbents with Different Amounts of Preadsorption and Desorption. The adsorbents with different preadsorption and desorption amounts of 0.0, 0.1,

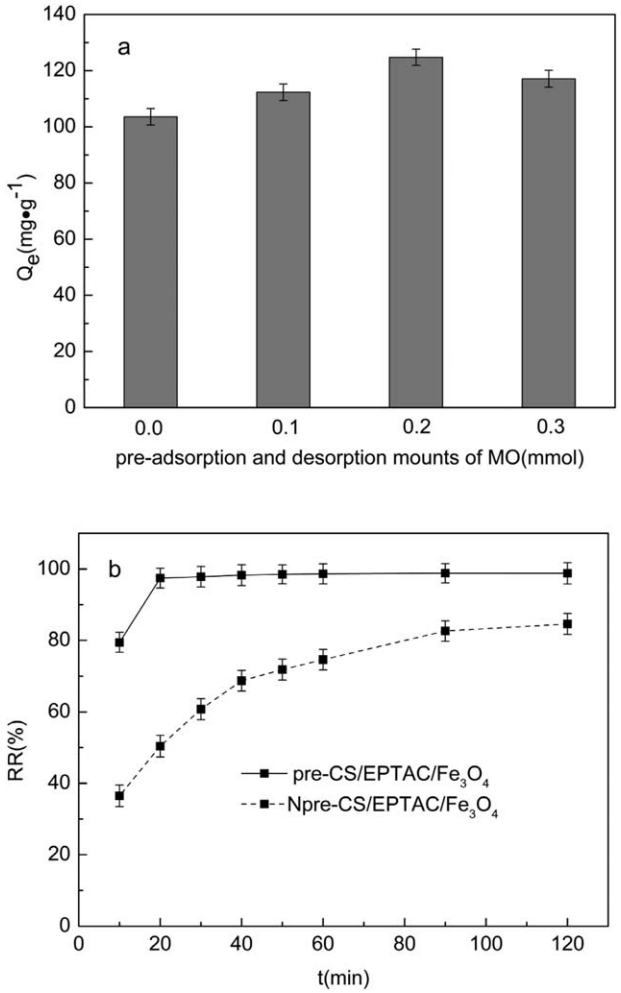

Figure 4. (a) Adsorption effect of the adsorbents with different preadsorption amounts of MO and (b) adsorption rate comparisons of pre-CS/EPTAC/Fe_3O_4 (with a 0.2 mmol preadsorption amount of MO) and Npre-CS/EPTAC/Fe_3O_4 for MO at 298 K. Adsorbent dose = 20 mg, initial MO concentration = 50 mg/L, solution volume = 50 mL, pH 3.0, and contact time = 120 min.

0.2, and 0.3 mmol MO were prepared in accordance with the previous method. The adsorption comparisons of MO onto the adsorbents were carried out with pH 3.0 at an initial MO concentration of 50 mg/L and an adsorbent dose of 20 mg/50 mL for 120 min. Figure 4(a) clearly showed a sharp increase in Q_e with increasing MO amount from 0.0 to 0.2 mmol, and a slight decrease in Q_e with increasing MO amount from 0.2 to 0.3 mmol. The result indicates that the optimum uptake was acquired at 0.2 mmol and the maximum Q_e was found to be 139.8 mg/g. In addition, the adsorption rate curves of pre-CS/EPTAC/Fe_3O_4 (with a 0.2-mmol preadsorption amount of MO) and Npre-CS/EPTAC/Fe_3O_4 are shown in Figure 4(b). It was obvious from our observations that the adsorption of MO onto pre-CS/EPTAC/Fe_3O_4 approached equilibrium at 20 min and remained constant for the following 120 min; this was much faster than Npre-CS/EPTAC/Fe_3O_4 (120 min). The removal rate of adsorption equilibrium of pre-CS/EPTAC/Fe_3O_4 (98.8%) was higher than that of Npre-CS/EPTAC/Fe_3O_4 (84.6%). From the previous discussion of SEM, the cavities on the pre-CS/EPTAC/Fe_3O_4 surface increased the adsorbent-specific surface area and further improved the absorption performance.

Adsorption Kinetics. The adsorption kinetic curves were obtained at pH 3.0 and C_0's of 20, 40, 60, and 80 mg/L. Figure 5 shows the adsorption kinetic curves of MO onto pre-CS/EPTAC/Fe_3O_4. We found that the adsorption process of MO onto pre-CS/EPTAC/Fe_3O_4 was relatively fast. The adsorption increased sharply from 0 to 20 min and then gradually decreased until the adsorption equilibrium approached (at 120 min). Additionally, an obvious increase in the initial concentrations of MO extended the adsorption equilibrium times; this suggested the dye concentration was also an important factor influencing the adsorption rate. To obtain the adsorption information of MO onto pre-CS/EPTAC/Fe_3O_4, pseudo-first-order [eq. (3)] and pseudo-second-order [eq. (4)] were used to fit the experimental data. The linear forms of the two models are expressed as follows[32]:

$$\lg(Q_e - Q_t) = -\frac{K_1 t}{2.303} + \lg Q_e \quad (3)$$

$$\frac{t}{Q_t} = \frac{1}{Q_e} t + \frac{1}{K_2 Q_e^2} \quad (4)$$

where Q_t is the dye amount adsorbed at time t (mg/g); K_1 (min^{-1}) and K_2 (g·mg^{-1}·min^{-1}) are the rate constants of pseudo-first-order and pseudo-second-order models, respectively; and t is the time (min).

The linearized forms of pseudo-first-order and pseudo-second-order kinetics model are given in Figure 6. Table I shows the fitting results obtained from two models. As indicated in Table I, the correlation coefficients (R^2s) of the pseudo-second-order model (0.9992–0.9998) were higher than those of the pseudo-first-order model (0.8576–0.9610). The measured equilibrium adsorption capacity values of Q_e' (49.4, 97.9, 145.5, and 187.2 mg/g) obtained through the experiments were close to the values of Q_e (50.2, 101.0, 151.5, and 196.1 mg/g) calculated with the pseudo-second-order model equation. Thus, the pseudo-

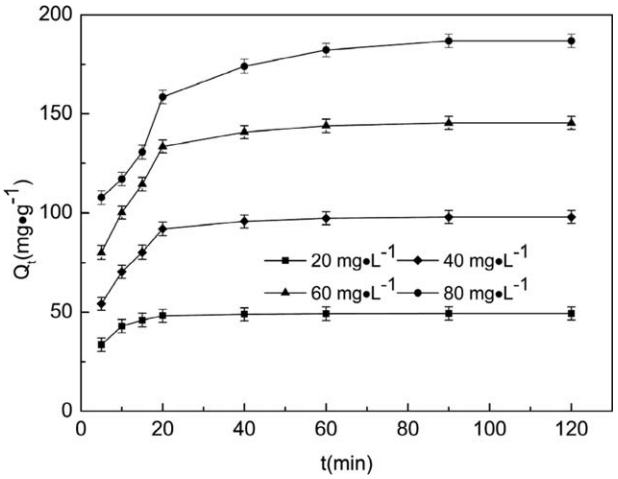

Figure 5. Adsorption curves for different concentrations of MO on pre-CS/EPTAC/Fe_3O_4 at 298 K. Adsorbent dose = 20 mg, solution volume = 50 mL, pH 3.0, and contact time = 120 min.

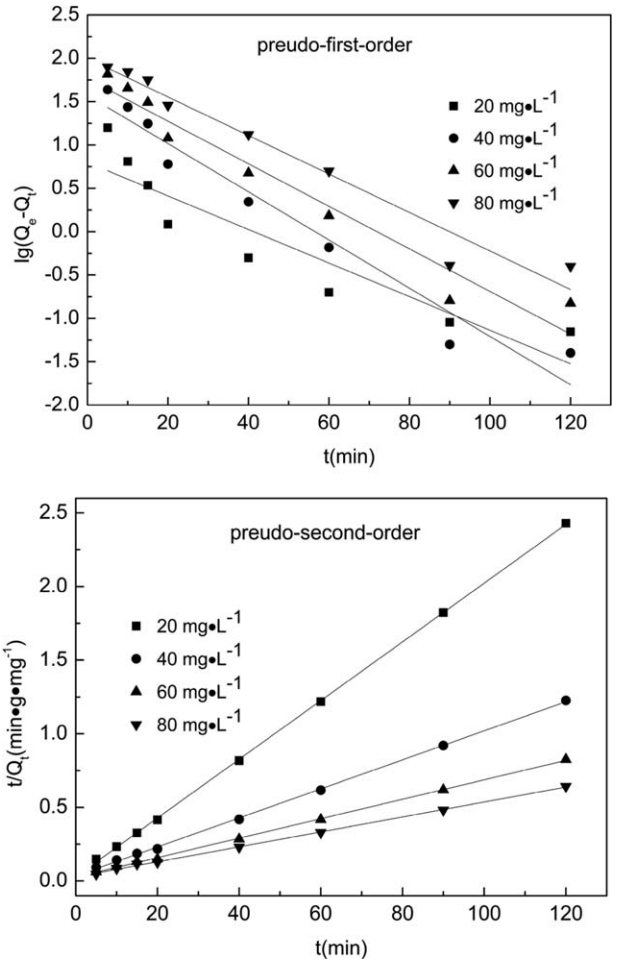

Figure 6. Pseudo-first-order and pseudo-second-order for the adsorption of MO on pre-CS/EPTAC/Fe_3O_4 at 298 K.

second-order model was suitable for describing the adsorption kinetic behavior. In addition, K_2 decreased gradually with increasing MO concentration. This may have been because the adsorption competition of MO molecules at lower concentrations was smaller than the competition at higher concentrations. Consequently, the adsorption rate was decreased.[33]

Adsorption Isotherms. The adsorption of MO onto pre-CS/EPTAC/Fe_3O_4 at pH 3.0 for C_0's ranging from 20 to 200 mg/L was performed for 120 min to reach the equilibrium state. To study the adsorption mechanism and evaluate the adsorption properties of pre-CS/EPTAC/Fe_3O_4, the Langmuir [eq. (5)] and

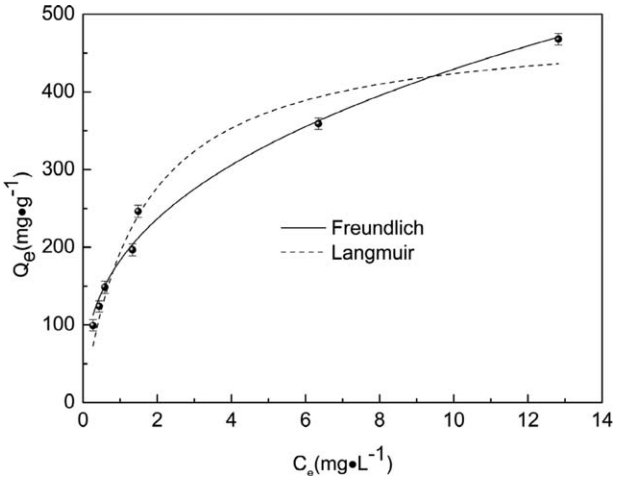

Figure 7. Adsorption isotherms of the pre-CS/EPTAC/Fe_3O_4 for MO at 298 K. Adsorbent dose = 20 mg, solution volume = 50 mL, pH 3.0, and contact time = 120 min.

Freundlich [eq. 6] models were used for adsorption isotherms. The Langmuir model assumes monolayer and homogeneous adsorption onto a surface with no interaction between the adsorbate molecules. The Freundlich model assumes multilayer adsorption onto heterogeneous surfaces with interaction between the adsorbed molecules. The equations of the adsorption isotherm could be expressed as follows[34]:

$$Q_e = \frac{Q_m K_L C_e}{1 + K_L C_e} \quad (5)$$

$$Q_e = K C_e^{1/n} \quad (6)$$

where Q_m is the maximum capacity (mg/g); K_L (L/mg) and K [mg/g·(L/mg)$^{1/n}$] are the Langmuir and Freundlich isotherm constants, respectively; and n is the heterogeneity factor.

Figure 7 shows the adsorption isotherms of MO on pre-CS/EPTAC/Fe_3O_4. The calculated K_L and K values are summarized in Table II. It was obvious that the Freundlich isotherm had a higher R^2 value (0.9810) than the Langmuir isotherm ($R^2 = 0.9613$); this indicated that the adsorption on the surface of pre-CS/EPTAC/Fe_3O_4 was multilayer adsorption. This was because, in addition to the electrostatic attraction between MO and pre-CS/EPTAC/Fe_3O_4, there were other forces, such as van der Waals forces, hydrogen bonding, and coordination effects. K [179.1 mg/g·(L/mg^{-1})$^{1/n}$] reached high values; this represented the greater binding capacity between MO and pre-CS/EPTAC/Fe_3O_4. Additionally, the value of $1/n$ (0.38) was less than 1; this suggested that the adsorption of MO on pre-CS/EPTAC/Fe_3O_4

Table I. Kinetic Parameters of MO Adsorption on Pre-CS/EPTAC/Fe_3O_4 at 298 K

		Pseudo-first-order			Pseudo-second-order		
C_0 (mg/L)	Q_e' (mg/g)	$K_1 \times 10^3$ (min^{-1})	Q_e (mg/g)	R^2	$K_2 \times 10^3$ (g·mg^{-1}·min^{-1})	Q_e (mg/g)	R^2
20	49.4	44.7	6.3	0.8576	683.8	50.2	0.9998
40	97.9	64.0	37.4	0.9576	293.8	101.0	0.9995
60	145.5	56.4	58.2	0.9524	250.9	151.5	0.9995
80	187.2	51.1	99.6	0.9610	178.9	196.1	0.9992

Table II. Fitting Results of the Adsorption Isotherm with the Langmuir and Freundlich Equations at 298 K

	Langmuir			Freundlich		
Dye	Q_m (mg/g)	$K_L \times 10^3$ (L/mg)	R^2	K [mg/g·(L·mg^{-1})$^{1/n}$]	$1/n$	R^2
MO	486.1	667.8	0.9613	179.1	0.38	0.9810

Table III. Comparison of the Adsorption Capacity of Pre-CS/EPTAC/Fe_3O_4 with Those of Different Adsorbent Materials

Adsorbent	Adsorption capacity (mg/g)	Reference
Chitosan/clay/Fe_3O_4	149.3	Cho *et al.*[35]
Chitosan/organicrectorite-Fe_3O_4 composite microspheres	5.6	Zeng *et al.*[36]
Chitosan/Al_2O_3/magnetic iron oxide nanoparticle composite	417.0	Tanhaei *et al.*[37]
Magnetic maghemite/chitosan nanocomposite films	28.9	Jiang *et al.*[2]
Chitosan enwrapping nanosized γ-Fe_2O_3 and MWCNTs	66.1	Zhu *et al.*[38]
HEMA-chitosan-MWCNT nanocomposite	306.0	Mahmoodian *et al.*[39]
Pre-CS/EPTAC/Fe_3O_4	486.1	This study

MWCNT, multiwalled carbon nanotube.

was favorable. The maximum adsorption capacity calculated with the Langmuir isotherm was 486.1 mg/g for MO. Compared to the other chitosan-based adsorbents for MO adsorption presented in Table III, the maximum adsorption capacity of pre-CS/EPTAC/Fe_3O_4 had a much higher value for MO uptake. The gained knowledge will contribute a new idea for modification to improve the adsorbent characteristics and performance.

Adsorption Thermodynamics. Thermodynamic parameters related to the intrinsic energy change of the adsorption, such as standard free energy change (ΔG; kJ/mol), enthalpy change (ΔH; kJ/mol), and entropy change (ΔS; J mol^{-1}·K^{-1}), are usually calculated according to eqs. (7) and 8:

$$\ln K = \frac{\Delta H}{RT} + \frac{\Delta S}{R} \quad (7)$$

$$\Delta G = \Delta H - T\Delta S \quad (8)$$

where T is the temperature (K), R (8.314 J·mol^{-1}·K^{-1}) is the universal gas constant, and K is the thermodynamic equilibrium constant for the adsorption, which can be obtained from the ratio of Q_e to C_e.

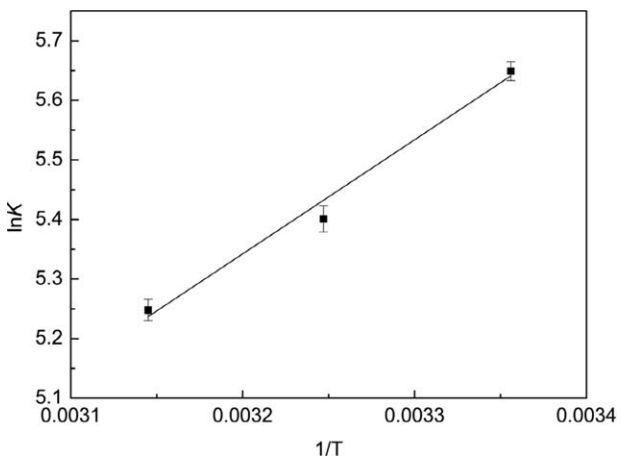

Figure 8. ln $K \approx 1/T$ plots for MO adsorption on pre-CS/EPTAC/Fe_3O_4.

The obtained ln K–$1/T$ plots and thermodynamic parameter values are shown in Figure 8 and Table IV, respectively. The negative ΔG values in the entire temperature range (298–318 K) demonstrated the MO dye adsorption was a exothermic and spontaneous process. Also, the less negative ΔG at high temperature suggested that the adsorption process was more spontaneous at low temperature. The negative ΔH (−15.8 kJ/mol) indicated the exothermic nature of adsorption. Furthermore, the negative ΔS (−6.3 J·mol^{-1}·K^{-1}) revealed the decreased randomness at the adsorbent–adsorbate interface during the fixation of MO on the active sites of the pre-CS/EPTAC/Fe_3O_4.

Adsorption for Other Azo Dyes. It is well known that azo dyes have similar molecular structures; this can result in similar adsorption behaviors on adsorbents. Figure 9 shows the adsorption performances of pre-CS/EPTAC/Fe_3O_4 and Npre-CS/EPTAC/Fe_3O_4 for AR1 and OG in 50-mL 50 mg/L solutions at pH 3.0. Obviously, the equilibrium removal rates of pre-CS/EPTAC/Fe_3O_4 for AR1 and OG were both about 98.0%. These values were higher than those of Npre-CS/EPTAC/Fe_3O_4 (92.7 and 85.6%); this suggested a good adsorption performance for pre-CS/EPTAC/Fe_3O_4.

With the method of preadsorption and desorption to prepare pre-CS/EPTAC/Fe_3O_4, we not only retained the characteristic groups of quaternary chitosan salt but also increased the specific

Table IV. Thermodynamic Parameters at Different Temperatures

Dye	T (K)	ΔG (kJ/mol)	ΔH (kJ/mol)	ΔS (J·mol^{-1}·K^{-1})
	298	−13.92		
MO	308	−13.86	−15.8	−6.3
	318	−13.80		

surface area of material. The adsorption performance of pre-CS/EPTAC/Fe_3O_4 for MO and other azo dyes with similar structures was greatly improved.

Recycling Experiments. From a practical application point, the recycling availability is a crucial evaluation factor for an excellent adsorbent. Gorensek's[40] research showed that a high temperature (>333 K) and high pH (>10.0) may affect the hydrolysis of reactive dyes and the adsorption. At the same time, the literature[41,42] has shown the adsorption difference of reactive dyes on adsorbents at different pHs could be used as the basis of adsorbent regeneration. Preliminary research results show that the electrostatic forces between the magnetic particles and dyes abated under alkaline conditions, the adsorption capacity was small, and the removal rate was low. Therefore, the saturated adsorbents were released and regenerated under alkaline conditions.

Desorption of pre-CS/EPTAC/Fe_3O_4 loaded MO was demonstrated with 20% NaOH aqueous solutions. The percentage of MO desorbed reached 95.0%. The adsorption–desorption of MO was conducted for six cycles. The results are illustrated in Figure 10. The adsorption efficiency of pre-CS/EPTAC/Fe_3O_4 remained almost constant (98.5%) for six cycles; this indicated that there were no irreversible sites on the adsorbent surface and pre-CS/EPTAC/Fe_3O_4 had an excellent regeneration performance.

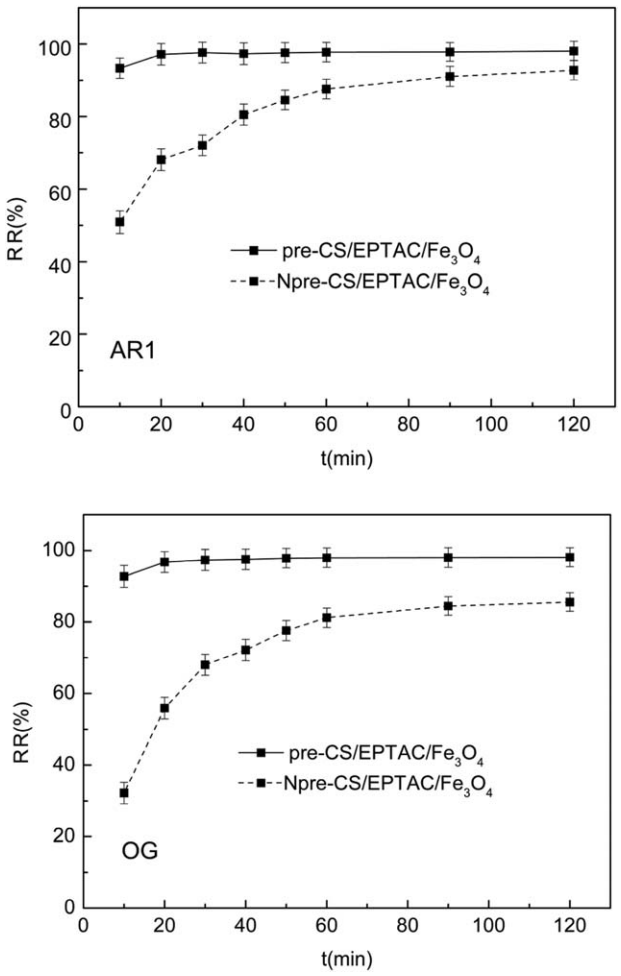

Figure 9. Adsorption rate comparisons of pre-CS/EPTAC/Fe_3O_4 and Npre-CS/EPTAC/Fe_3O_4 for AR1 and OG at 298 K. Adsorbent dose = 20 mg, C_0 = 50 mg/L, solution volume = 50 mL, pH 3.0, and contact time = 120 min.

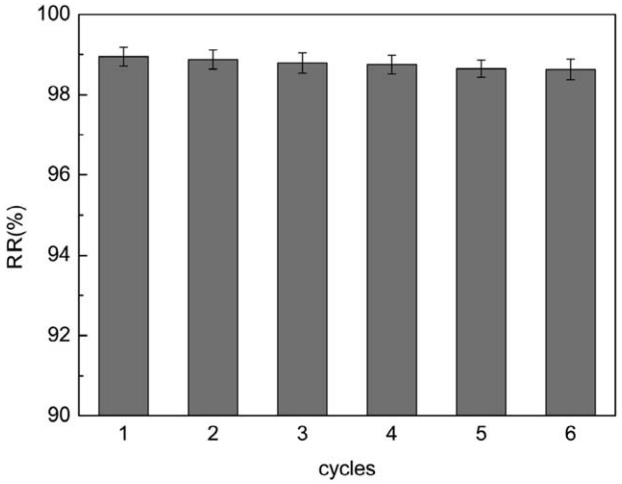

Figure 10. Recycling experiments for MO removal at 298 K. Adsorbent dose = 20 mg, initial MO concentration = 50 mg/L, solution volume = 50 mL, pH 3.0, and contact time = 120 min.

CONCLUSIONS

In this study, pre-CS/EPTAC/Fe_3O_4, a kind of efficient and easily recycled adsorbent, was prepared by a novel method and characterized by several methods, and the adsorption properties of pre-CS/EPTAC/Fe_3O_4 for MO and other azo dyes were researched.

We found that the preadsorption and desorption of MO played an important role in the adsorption of MO in aqueous solution. The amount of MO of preadsorption and desorption influenced the material morphology and adsorption effect. The optimum removal rate was acquired at 0.2 mmol of MO. The adsorption of MO onto pre-CS/EPTAC/Fe_3O_4 was rapid and approached equilibrium at 20 min; this was much faster than Npre-CS/EPTAC/Fe_3O_4 (120 min). The kinetics and isotherm of MO onto pre-CS/EPTAC/Fe_3O_4 were described by the pseudo-second-order and Freundlich isotherm model, respectively. The maximum adsorption capacity calculated with the Langmuir isotherm was 486.1 mg/g for MO. In addition, various thermodynamic parameters, such as ΔG, ΔH, and ΔS, were calculated; these showed adsorption to be a spontaneous and exothermic process. For other azo dyes with similar structures, such as AR1 and OG, the adsorption efficiency was greatly improved. Furthermore, pre-CS/EPTAC/Fe_3O_4 could be rapidly separated by an external magnetic field and efficiently regenerated by the 20% NaOH aqueous solution treatment. This treatment retained a high removal efficiency in six successive cycles; this suggests their potential application values in practical water treatment.

ACKNOWLEDGMENTS

This work was financially supported by the Public Research Fund of Science and Technology Department of Liaoning Province (contract grant number 2015003005) and the Key Laboratory Project of Shenyang Science and Technology Bureau (contract grant number F15-154-1-00).

REFERENCES

1. Olya, M. E.; Pirkarami, A.; Mirzaie, M. *Chemosphere* **2013**, *91*, 935.
2. Jiang, R.; Fu, Y. Q.; Zhu, H. Y.; Yao, J.; Xiao, L. *J. Appl. Polym. Sci.* **2012**, *125*, 540.
3. Gao, H. J.; Kan, T. T.; Zhao, S. Y.; Qian, Y. X.; Cheng, X. Y.; Wu, W. L.; Wang, X. D.; Zheng, L. Q. J. *Hazard. Mater.* **2013**, *261*, 83.
4. Dong, Y.; Lin, H.; Qu, F. *Chem. Eng. J.* **2012**, *193–194*, 169.
5. Punzi, M.; Anbalagan, A.; Börner, R. A.; Svensson, B. M.; Jonstrup, B. M. *Chem. Eng. J.* **2015**, *270*, 290.
6. Morshedi, D.; Mohammadi, Z.; Akbar Boojar, M. M.; Aliakbari, F. *Colloids Surfaces B* **2013**, *112*, 245.
7. Xu, L. L.; Li, X. F.; Ma, J. Q.; Wen, Y. Z.; Liu, W. P. *Appl. Catal. A* **2014**, *485*, 91.
8. Sun, J.; Yan, X.; Lv, K. L.; Sun, S.; Deng, K. J.; Du, D. Y. *J. Mol. Catal. A* **2013**, *367*, 31.
9. Zavastin, D. E.; Gherman, S.; I. Cretescu. *Rev. Chim.* **2012**, *63*, 1075.
10. Labanda, J.; Sabaté, J.; Llorens, J. *J. Chem. Eng. J.* **2011**, *166*, 536.
11. Mane, V. S.; Vijay Babu, P. V. *J. Taiwan Inst. Chem. E.* **2013**, *44*, 81.
12. Cheah, W.; Hosseini, S.; Khan, M. A.; Chuah, T. G.; Choong, T. S. Y. *Chem. Eng. J.* **2013**, *215–216*, 747.
13. Kyzas, G. Z.; Deliyanni, E. A.; Lazaridis, K. N. *J. Colloid Interface Sci.* **2014**, *430*, 166.
14. Greluk, M.; Hubicki, Z. *Desalination* **2011**, *278*, 219.
15. Panic, V. V.; Velickovic, S. *J. Sep. Purif. Technol.* **2014**, *122*, 384.
16. Chen, H.; Zhong, A. G.; Wu, J. Y.; Zhao, J.; Yan, H. *Ind. Eng. Chem. Res.* **2012**, *51*, 14026.
17. Lin, S.; Wei, W.; Wu, X. H.; Zhou, T.; Mao, J.; Yun, Y. S. *J. Hazard. Mater.* **2015**, *299*, 10.
18. Sheshmani, S.; Ashori, A.; Hasanzadeh, S. *Int. J. Biol. Macromol.* **2014**, *68*, 218.
19. Wan Ngah, W. S.; Teong, L. C.; Hanafiah, M. A. K. M. *Carbohydr. Polym.* **2011**, *83*, 1446.
20. Liu, L.; Li, C.; Bao, C. L.; Jia, Q.; Xiao, P. F.; Liu, X. T.; Zhang, Q. P. *Talanta* **2012**, *93*, 350.
21. ELwakeel, K. Z. *J. Hazard. Mater.* **2009**, *167*, 383.
22. Atia, A. A.; Donia, A. M.; ELwakeel, K. Z. *J. Hazard. Mater.* **2008**, *151*, 372.
23. Cao, C. H.; Xiao, L.; Chen, C. H.; Shi, X. W.; Cao, Q. H.; Gao, L. *Powder Technol.* **2014**, *260*, 90.
24. Zhou, Z. K.; Lin, S. Q.; Yue, T. L.; Lee, T. C. *J. Food Eng.* **2014**, *126*, 133.
25. Fan, L. L.; Luo, C. N.; Sun, M.; Li, X. J.; Lu, F. G.; Qiu, H. M. *Bioresour. Technol.* **2012**, *114*, 703.
26. Zhou, L. M.; Shang, C.; Liu, Z. R. *Acta Phys.-Chim. Sin.* **2011**, *27*, 677.
27. Zhang, C. L.; Hou, X. H.; Liang, N.; Ding, Y. Y.; Hu, X. M. *Water Sci. Technol.* **2014**, *70*, 649.
28. Zhu, H. Y.; Fu, Y. Q.; Jiang, R.; Yao, J.; Xiao, L.; Zeng, G. M. *Bioresour. Technol.* **2012**, *105*, 24.
29. Kyzas, G. Z.; Lazaridis, N. K.; Bikiaris, D. N. *Carbohydr. Polym.* **2013**, *91*, 198.
30. Vachoud, L.; Chen, T.; Payne Rafael, G. F. V. D. *Enzyme Microb. Tech.* **2001**, *29*(6–7), 380.
31. Zhang, X.; Jiao, C.; Wang, J.; Liu, Q.; Li, R.; Yang, P.; Zhang, M. *Chem. Eng. J.* **2012**, *198–199*, 412.
32. Lian, L. L.; Cao, X. L.; Wu, Y. Q.; Lou, D. W.; Han, D. D. *J. Taiwan Inst. Chem. E* **2013**, *44*, 67.
33. Zhang, J. X.; Zhou, Q. X.; Ou, L. L. *J. Chem. Eng. Data* **2012**, *57*, 412.
34. Mahmoodi, N. M. *J. Taiwan Inst. Chem. E.* **2013**, *44*, 322.
35. Cho, D. W.; Jeon, B. H.; Chon, C. M.; Schwartz, F. W.; Jeong, Y.; H. Song. *J. Ind. Eng. Chem.* **2015**, *28*, 60.
36. Zeng, L. X.; Xie, M. J.; Zhang, Q. Y.; Kang, Y.; Guo, X. M.; Xiao, H. J.; Peng, Y. N.; Luo, J. W. *Carbohydr. Polym.* **2015**, *123*, 89.
37. Tanhaei, B.; Ayati, A.; Lahtinen, M.; Sillanpaa, M. *Chem. Eng. J.* **2015**, *259*, 1.
38. Zhu, H. Y.; Jiang, R.; Xiao, L.; Zeng, G. M. *Bioresour. Technol.* **2010**, *101*, 5063.
39. Mahmoodian, H.; Moradi, O.; Shariatzadeha, B.; Salehf, T. A.; Tyagi, I.; Maity, A.; Asif, M.; Gupta, V. K. *J. Mol. Liq.* **2015**, *202*, 189.
40. Gorensek, M. *Dyes Pigments* **1999**, *40*, 225.
41. Gu, Y. X.; Song, P.; Li, T.; Sui, W. P. *Carbohydr. Res.* **2011**, *346*, 769.
42. Zhou, L. M.; Xu, J. P.; Liu, Z. R.; Shang, C.; Hang, G. L. *Polym. Mater. Sci. E* **2012**, *28*, 142–145 and 150.